Resistive Interchange Modes Destabilized by Helically Trapped Energetic Ions in a Helical Plasma

X. D. Du,[1,*] K. Toi,[2] M. Osakabe,[1,2] S. Ohdachi,[1,2] T. Ido,[2] K. Tanaka,[2] M. Yokoyama,[1,2] M. Yoshinuma,[1,2] K. Ogawa,[2] K. Y. Watanabe,[2] M. Isobe,[1,2] K. Nagaoka,[1,2] T. Ozaki,[2] S. Sakakibara,[1,2] R. Seki,[2] A. Shimizu,[2] Y. Suzuki,[1,2] H. Tsuchiya,[2] and LHD Experiment Group

[1]*Department of Fusion Science, The Graduate University for Advanced Study, 509-5292 Toki, Japan*
[2]*National Institute for Fusion Science, 509-5292 Toki, Japan*

(Received 20 June 2014; revised manuscript received 18 January 2015; published 17 April 2015)

A new bursting $m = 1/n = 1$ instability (m, n: poloidal and toroidal mode numbers) with rapid frequency chirping down has been observed for the first time in a helical plasma with intense perpendicular neutral beam injection. This is destabilized in the plasma peripheral region by resonant interaction between helically trapped energetic ions and the resistive interchange mode. A large radial electric field is induced near the edge due to enhanced radial transport of the trapped energetic ions by the mode, and leads to clear change in toroidal plasma flow, suppression of microturbulence, and triggering an improvement of bulk plasma confinement.

DOI: 10.1103/PhysRevLett.114.155003 PACS numbers: 52.35.Py, 52.55.Hc, 52.55.Pi

Good confinement of energetic ions (EPs) such as alpha particles is crucial for sustaining deuterium-tritium burning plasma. This may be threatened by magnetohydrodynamic (MHD) instabilities destabilized by resonant interactions between EPs and marginally stable or weakly unstable eigenmodes. Interesting and important results on instabilities driven by passing EPs are reported from many tokamak and helical devices [1]. On the other hand, so-called fishbone (FB) instability destabilized by trapped EPs was detected in a tokamak plasma three decades ago [2]. Recently, FB study has been expanded to the so-called energetic particle driven wall mode (EWM) or off-axis fishbone instability, which is also destabilized by trapped EPs [1,3–5]. Much attention is paid to the mode toward the burning plasma experiments because it often triggers the resistive wall mode and disruption. Recently, a bursting mode exhibiting rapid frequency chirping has been newly observed during perpendicular neutral beam injection (PERP-NBI) on the Large Helical Device (LHD). This mode is destabilized by resonant interaction between helically trapped EPs and the resistive interchange mode (RIC) localized at the mode rational surface. Hereafter, this mode is called the "EIC" (energetic ion driven resistive interchange mode). Also, in a tokamak, the RIC can be destabilized having a localized mode character at the mode rational surface in the negative central magnetic shear region of a reversed shear plasma with high normalized beta [6,7]. The burst often triggers major disruption. Interaction of the RIC with trapped EPs would be more dangerous in a future large tokamak. This Letter reports the characteristics of the EIC and the impacts on helical plasmas. Interaction between trapped EPs and the RIC is a very important topic for tokamak plasmas as well as helical plasmas in the future.

The EIC is typically observed in relatively low density plasmas of the line averaged electron density $\langle n_e \rangle = 0.5\text{–}1.5 \times 10^{19}$ m^{-3} at high toroidal field strength $B_t = 2.5\text{–}2.85$ T in the LHD. In the plasmas, three tangential hydrogen beam lines with initial beam energy $E_b \sim 180$ keV and two perpendicular beam lines (PERP-NBI) with $E_b \sim 34$ keV are employed. A typical magnetic probe (MP) signal of the $m = 1/n = 1$ EIC is shown in Fig. 1. The EIC grows rapidly (<0.2 ms) and reaches the very large amplitude of ~3 G at the MP position, having a strongly distorted oscillatory waveform. The initial frequency is around 9 kHz and quickly chirps down to ~3.5 kHz in the laboratory frame. The Doppler frequency due to toroidal and poloidal rotations at the $\iota = 1$ surface (ι: rotational transform) is small as $f_{\rm pol} + f_{\rm tor} = 0.4$ kHz, estimated from the carbon impurity emission measured

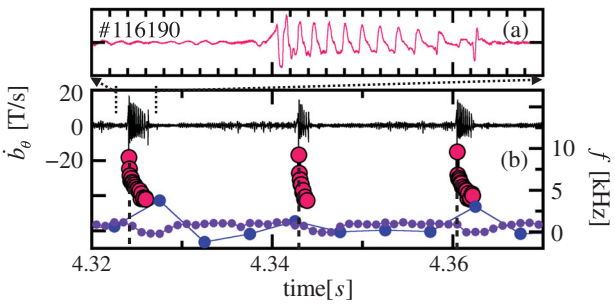

FIG. 1 (color). (a) The zoomed waveform of EIC magnetic fluctuations. (b) Three EIC bursts, the temporal frequencies (red), and the toroidal (purple) and poloidal (blue) rotation frequencies at the $\iota = 1$ surface, measured by CXRS.

by charge exchange recombination spectroscopy (CXRS) [8]. The mode propagates in the electron diamagnetic drift (EDD) direction poloidally and counter-B_t direction toroidally, in the plasma frame. The negative sign of the frequency in Fig. 1(b) stands for the counter-B_t direction and ion diamagnetic drift (IDD) direction poloidally.

Since EICs are excited by injection of PERP-NBI, the drift orbits of helically trapped EPs are calculated for the vacuum field by a Lorentz orbit simulation code [9] to clarify the relation between the observed mode frequency and the orbit frequencies. A test proton of E_b=34 keV and the pitch angle $\chi = 85°$ is launched at various radial positions and tracked numerically. The orbit shown in Fig. 2(a) consists of two parts: rapid bounce motions in a narrow helical-ripple well having weak magnetic field strength of the $l/N = 2/10$ helical pitch (l: polarity of the helical field, N: toroidal period number) and a helical excursion along the well. The proton travels in the counter-B_t direction toroidally and the IDD direction poloidally. It circulates around the torus, similar to the motion of the passing particles in a tokamak, and is confined well in the helical-ripple well. The poloidal precession frequencies $\langle f_\theta^{\rm EP}\rangle$ vary from -3.6 to -11 kHz in the region $0.4 \le r/a \le 1$ (a: averaged minor radius). The toroidal precession frequency $\langle f_\zeta^{\rm EP}\rangle$ is one fifth ($=l/N$) of $\langle f_\theta^{\rm EP}\rangle$, as shown in Fig. 2(b). The resonance condition between the MHD mode and EPs in a helical plasma is given as $f_{\rm res} - (m + j\mu)\langle f_\theta^{\rm EP}\rangle + (n + j\nu N)\langle f_\zeta^{\rm EP}\rangle = 0$, where $j = 0$ or ± 1 [10]. This equation expresses the condition that the MHD mode having a $\cos(m\theta - n\zeta)$ structure resonates with the toroidal drift velocity of the EPs having a $\cos(\mu\theta - \nu N\zeta)$ structure over a long time period. The case of $j = 0$ recovers the resonant condition for a tokamak plasma. For LHD plasmas, the resonance frequency is evaluated as $f_{\rm res} = -1.2\langle f_\theta^{\rm EP}\rangle$ for $j = 1$, $\nu = 1$, and $\mu = 0$. This indicates that the EIC excited by the resonance would propagate opposite to the poloidal precession direction and in the same direction as the toroidal precession of helically trapped EPs, which is also seen from Fig. 2(a). This is consistent with the experimental observation. Since $\langle f_\theta^{\rm EP}\rangle$ at the $\iota = 1$ surface is -6.9 kHz, the $f_{\rm res} = +8.3$ kHz agrees well with the observed frequency $+8.6$ kHz in the plasma frame. Note that PERP-NBI is always necessary to excite the EIC and the charge exchanged neutral flux measured perpendicular to the toroidal field [11] indicates clear resonant interaction between the EIC and 34 keV beam ions.

Figure 3 shows time evolution of electron temperature fluctuation $\tilde{T}_e$ measured by electron cyclotron emission (ECE) [12] and the derived eigenfunctions of the MHD modes. The radial displacement ξ_r is evaluated as $\tilde{T}_e/(-\nabla T_e)$ (∇T_e: gradient of the electron temperature), where the conditional averaging is applied to several crests and troughs of the $\tilde{T}_e$ waveform. In phase I, the $m = 1/n = 1$ MHD mode of ~3.5 kHz is weakly destabilized. The mode propagates in the EDD direction in the plasma frame, a fact that is recognized in many LHD shots [13]. The RIC is easily destabilized by the pressure gradient in the plasma edge region of a LHD plasma, because the edge region is in a magnetic hill. The ξ_r strongly localizes at the $\iota = 1$ rational surface of $r/a \sim 0.88$ with an even function, as shown in Fig. 3(c). The observed ξ_r is similar to the ξ_r of the unstable RIC calculated for a cylindrical plasma of magnetic Reynolds number $S = 1 \times 10^6$ by a linear global resistive MHD code [14], which is shown with broken curves in Fig. 3(c). The mode is thought to be RIC. Note that the stability of the above plasma against the ideal interchange mode is assessed to be stable by the Mercier criterion. This assessment is experimentally confirmed in LHD [15]. In phase II, the $\tilde{T}_e$ extends radially inward,

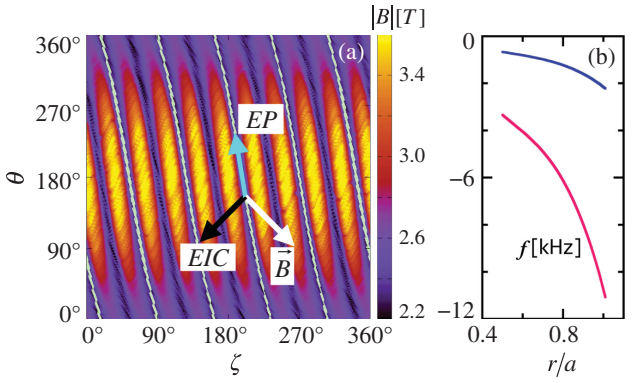

FIG. 2 (color). (a) Contour of the magnetic field strength $|B|$ and the orbit of helically trapped fast ions at the $\iota = 1$ surface. The arrows indicate the directions of the magnetic field line, drift orbits, and mode propagation. (b) Profile of the calculated toroidal (blue) and poloidal (red) precession frequencies of the trapped EPs, where the $\iota = 1$ surface is at $r/a \sim 0.85$–0.88.

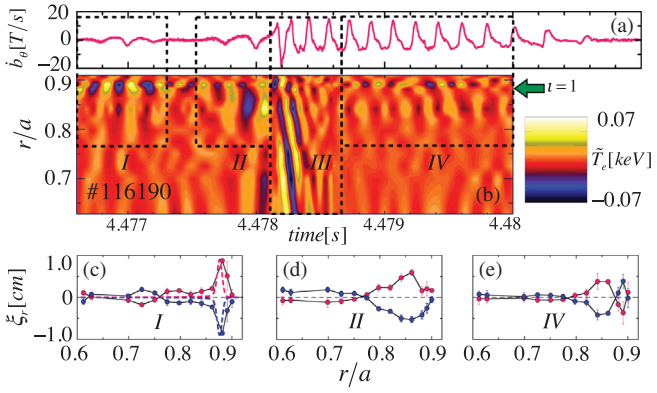

FIG. 3 (color). Time evolutions of the magnetic probe signal with one typical EIC (a) and the electron temperature fluctuation $\tilde{T}_e$ profile (b). The conditional averaged radial displacements for each crest (blue) and trough (red) of $\tilde{T}_e$ in phases I, II, and IV [(c), (d), and (e)]. The calculated eigenfunction for the RIC is also shown with broken curves in (c).

accompanied by an appreciable increase of magnetic fluctuation amplitude. The ξ_r clearly expands radially, holding the RIC character, as shown in Fig. 3(d). The mode in phase *II* is thought to be RIC. In phase *III*, the mode frequency suddenly jumps up and rapidly chirps down, where the amplitude also rapidly increases and immediately saturates nonlinearly, exhibiting a bursting nature. As shown in Fig. 3(b), a complicated radial structure of $\tilde{T}_e$ develops rapidly, propagating inward. Then, it shrinks quickly around the $\iota = 1$ surface. In phase *IV*, the ξ_r of the EIC has an island-type structure, where it behaves with the π phase difference across the $\iota = 1$ surface, as shown in Fig. 3(e).

The temporal behaviors of the modes in phases *II* to *IV* are interpreted as follows. The radially expanded ξ_r in phase *II* is explained by flattening of the T_e profile around the $\iota = 1$ surface due to the growth of the RIC. The steepened pressure gradient just on the inward side of the flattened region would tend to expand the mode structure radially further. At the beginning of phase *III*, the EIC is suddenly destabilized. It will be triggered by the increased beta value of trapped EP pressure ($\beta_{\perp h}$ = EP pressure/magnetic pressure) beyond the threshold. The EIC is thought to be a new branch of the resistive interchange mode associated with the large population of the helically trapped EPs. The threshold is crudely estimated by the FIT3D code [16] to be $\beta_{\perp h} \sim 0.2\%$ at the mode rational surface in a specific shot, where $\beta_{\perp h}$ is gradually increased by gradually decreasing $\langle n_e \rangle$ with constant beam power. The strong EIC immediately flattens the T_e profile and presumably also the trapped EP pressure profile, enhancing radial transport of the EPs. This process would lead to steepening both bulk and EP pressure gradients just on the inward side of the flattened region. Because of a decreasing character of $\langle f_\theta^{\mathrm{EP}} \rangle$ toward the plasma center [Fig. 2(b)], slightly slowed-down EPs as well as the newly born EPs would resonate with RIC over the region radially extended inward. These processes will expand the mode structure radially inward in phase *III*. So far, the eigenfunction ξ_r in phase *III* cannot be derived reliably, due to the rapid and complex time evolutions of $\tilde{T}_e$ and ∇T_e. In the latter part of the phase, a sudden decrease of $\tilde{T}_e$ is interpreted by a noticeable reduction of ∇T_e in $0.8 \le r/a \le 0.9$ by the EIC. A shape of ξ_r in phase *IV* is similar to that in the usual RIC, of which island type ξ_r is found out in LHD plasmas experimentally [17] and theoretically [14,18].

Clear impacts of EICs on bulk plasma are observed. Each EIC induces a significant and uniform plasma potential drop $|\Delta\phi|$ up to 13 kV in a wide core region ($|r/a| \le 0.7$), as shown in Fig. 4(b). The $\Delta\phi$ profiles in $-0.4 \lesssim r/a \lesssim 0.9$ on the $R_{\mathrm{ax}} = 3.75$ m configuration and $0 \lesssim r/a \lesssim 0.6$ on the $R_{\mathrm{ax}} = 3.6$ m one (R_{ax}: magnetic axis position of the vacuum field) are respectively obtained by accumulated measurements for nearly identical bursts, using a 10 Hz radial beam scan of the Heavy Ion Beam Probe (HIBP)

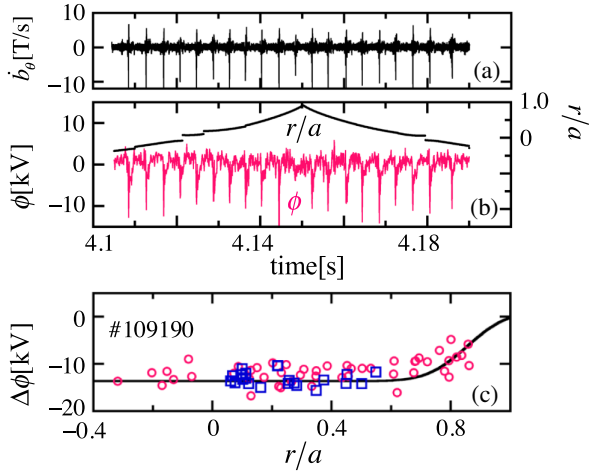

FIG. 4 (color online). Time evolutions of the magnetic probe signal (a) and the plasma potential ϕ obtained by a radial beam scan (r/a) of HIBP (b). Radial profile of the potential change during the EIC burst in $R_{\mathrm{ax}} = 3.75$ m (circles) in No. 109190 and 3.6 m (squares) configurations in No. 122476 and the fitted profile (solid curve) (c).

[19], shown in Fig. 4(c). This suggests a generation of negative radial electric field E_r near the plasma edge, which will be induced by nonambipolar transport of helically trapped EPs. The $\Delta\phi$ calculated by a model of $\Delta E_r = -85\exp[-((\rho - 0.85)/0.15)^2]$ kV/m is also shown in the solid curve.

Synchronizing with the potential change, strong modification of toroidal plasma flow is observed by CXRS. In Fig. 5, time evolutions of toroidal flow velocity V_ζ at $r/a \sim 0.85$ and plasma potential ϕ at $r/a \sim 0.1$ are shown as a function of the time defined by the onset of the EIC, τ_{EIC}.

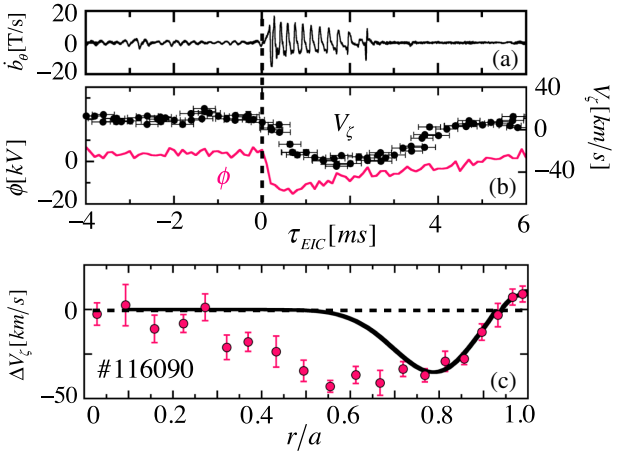

FIG. 5 (color online). Waveforms of the EIC burst (a) and the observed toroidal flow V_ζ and plasma potential ϕ (b), as a function of the relative time for the EIC onset. Radial profile of the V_ζ change (circles) and the calculated neoclassical flow (solid curve) at $\tau_{\mathrm{EIC}} = 2$ ms (c). Note that the potential waveform is measured in No. 122475 with one nearly identical EIC in (a).

The data points of V_ζ obtained every 1 ms are conditionally accumulated for nearly 10 events in a shot No. 116190 to obtain the clear time evolution statistically. The ϕ suddenly drops at $\tau_{\rm EIC} = 0$ ms, and recovers to the initial level in ~5 ms. Simultaneously, V_ζ starts to change and reaches the maximum change at $\tau_{\rm EIC} = 2$ ms. Then, it returns to the initial level ~3 ms after the burst. The flow change ΔV_ζ is shown in Fig. 5(c). While the V_ζ is enhanced in the counter-B_t direction in the core region ($0.3 \lesssim r/a \lesssim 0.9$), it is enhanced in the co-B_t direction in the very edge region ($0.9 \lesssim r/a \lesssim 1.0$). The ΔV_ζ can be explained by the neoclassical theory of net-current-free helical plasmas [20]:

$$\langle \vec{u}_I \cdot \nabla\zeta \rangle = \frac{1}{J}\left\{ -[\langle G_{BS}\rangle_i]\left(\frac{1}{e_i n_i}\frac{dP_i}{d\psi} + \frac{d\phi}{d\psi}\right) - \langle G_{BS}\rangle_i L_{54}^{*}\frac{1}{e_i}\frac{dT_i}{d\psi}\right\},$$

where $J \equiv RB_\phi$, $\psi \equiv r^2 B_\theta/2$, and $\langle G_{BS}\rangle_i$ is the geometric factor. The radial electric field ($d\phi/d\psi = \phi'$) can be expressed as $\phi' = \phi'_{\rm neo} + \phi'_{\rm EIC}$, where $\phi'_{\rm neo}$ and $\phi'_{\rm EIC}$ are the radial electric fields associated with neoclassical ambipolar potential and that induced by the EIC, respectively. Because $\phi'_{\rm EIC}$ is much larger than other terms, the expected V_ζ change can be obtained numerically from $\Delta\vec{u}_\zeta \approx -(R/J)^2(\langle G_{BS}\rangle_i/r)(d\phi_{\rm EIC}/dr)$ [21], employing $d\phi_{\rm EIC}/dr$ inferred from Fig. 4(c). The calculated result [a solid curve in Fig. 5(c)] agrees well with the observed ΔV_ζ at $\tau_{\rm EIC} = 2$ ms around the EIC location ($0.7 \lesssim r/a \lesssim 1.0$). In the present LHD plasma, the geometric factor $\langle G_{BS}\rangle_i$ changes the sign in the very edge region. This suggests the change of the sign of ΔV_ζ there by the EIC induced torque. In the inner region of $r/a \lesssim 0.7$, the calculated ΔV_ζ obviously deviates from the experimental results. This deviation will be due to the large radial diffusion caused by radial viscosity there. On the contrary, the viscosity in the edge will be substantially reduced due to clear suppression of microturbulence by the EIC, which will be discussed below.

The lower bound of the loss fraction of helically trapped EPs by the EIC can be estimated by a toroidal angular momentum balance, ignoring the viscosity term as $d\langle R_0 m_i n_i V_\zeta\rangle/dt \sim J_i \cdot \nabla\Psi_p$ [4]. The radial current density J_i responds to the orbit shift due to the EIC perturbation and the radial transport of EPs across the magnetic surfaces. For the orbit shift of $r_{\rm shift} \sim 0.15a$, estimated from the mode eigenfunction, $\Delta V_\zeta = 35$ km/s measured by CXRS, and helically trapped EP density $n_h/n_i \sim 2\%$–4% calculated by the FIT3D code, the loss fraction is estimated fairly large, i.e., $\langle n_h^{\rm loss}/n_h\rangle \sim (M_i/eB_p)(\Delta V_\zeta/r_{\rm shift})(n_h/n_i)^{-1} \sim$ 20%–40% estimated over the EIC mode region. A nearly comparable result is also estimated from the observed $\Delta\phi$ using $J_i \sim \varepsilon_0(\varepsilon_\perp - 1)\langle dE_r/dt\rangle$ [22], where $\varepsilon_\perp \sim (1 + q^2/\sqrt{\epsilon_h})(c/V_A)^2$ with the light speed c, Alfvén speed V_A, safety factor q and helical ripple ϵ_h. Moreover, the power loss by the lost EPs is estimated from the sudden drop of the stored energy ($W_{\rm dia}$) measured by a diamagnetic loop, which can detect the pressure of trapped EPs with $\chi \sim 90°$. The sudden drop of $dW_{\rm dia}/dt$ by the EIC indicates about a 15% to 30% loss of the total deposited power of PERP-NBI. That is, considerable loss of the trapped EPs controls the generation of the observed $\Delta\phi$ and ΔV_ζ.

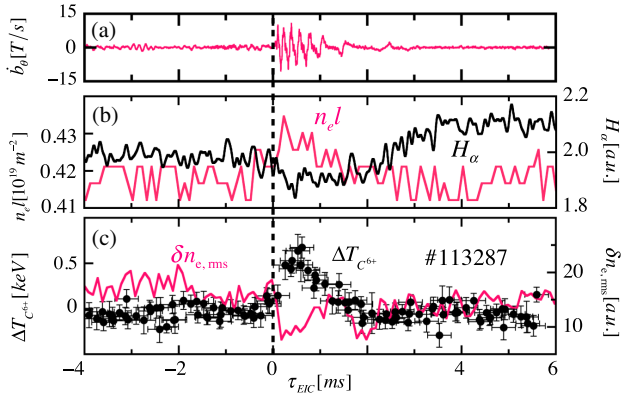

FIG. 6 (color online). Waveforms of the EIC burst (a), line integrated electron density $n_e l$ and H_α emission (b), and the increment of the C^{+6} ion temperature $\Delta T_{C^{+6}}$ and root-mean-squared density fluctuations $\delta n_{e,\rm rms}$ in the range of 20–500 kHz (c), as a function of the relative time for the EIC onset. Note that the $\Delta T_{C^{+6}}$ data points are obtained from 11 EIC events.

A noticeable reduction of H_α emission and a clear increase of the line electron density near the plasma edge are observed during the EIC, as shown in Figs. 6(a) and 6(b). The carbon ion (C^{+6}) temperature $T_{C^{+6}}$ also rises quickly (in ~0.6 ms) in the region of $0.6 \lesssim r/a \lesssim 1$. The temperature increment $\Delta T_{C^{+6}}$ obtained every 1 ms are conditionally accumulated for nearly identical 10 events in a shot No. 113287 to obtain the clear time evolution statistically. Note that the collisional relaxation time among C^{+6} ions of 1 keV is ~0.5 ms, where the C^{+6} ion density is 5% of $\langle n_e\rangle$. Simultaneously, clear suppression of density fluctuations $\delta n_{e,\rm rms}$ due to microturbulence is detected by a two-dimensional phase contrast imaging system [23], as shown in Fig. 6(c). The suppression takes place around $r/a \sim 0.85$ in the frequency range of 100–500 kHz and the perpendicular wave number normalized by the thermal ion gyroradius of $k_\perp \rho_{T_i} \sim 0.3$. The fluctuations in $0.5 \lesssim r/a \lesssim 1.0$ propagate in the IDD direction in the laboratory frame and peak at $r/a \sim 0.8$. According to a gyrokinetic simulation by GS2 code, the suppressed fluctuations are likely to be ion temperature gradient turbulence [24,25], of which the growth rate is around 1–2×10^5 s^{-1} for the present plasma parameters [25]. This is comparable to the $E \times B$ shearing rate of $\sim 2.5 \times 10^5$ s^{-1} induced by the EIC near the edge, of which the rate is estimated from the observed $\Delta\phi$ shown in Fig. 4(c). The generated sheared flow clearly reduces $\delta n_{e,\rm rms}$. The increased rate of the stored energy of the C^{+6} ion component (~0.47 MW) estimated from the

observed $\Delta T_{C^{+6}}$ does not contradict with the power input to C^{+6} ions of ~0.68 MW. The increases of $T_{C^{+6}}$ and n_e near the EIC location indicate transient improvement of bulk plasma confinement.

In summary, the $m = 1/n = 1$ MHD mode called the EIC, destabilized by helically trapped EPs has been observed for the first time in a helical plasma. The mode frequency is determined by the precession frequency of the EPs. The eigenfunction is localized at the mode rational surface (in this case, at the $\iota = 1$ surface), of which the localized mode character is similar to that of the usual pressure-driven RIC. Considerable amounts of EP losses lead to large E_r shear generation, which is confirmed by direct measurement of the plasma potential, and large toroidal flow change. The EIC generated E_r shear triggers transient confinement improvement of bulk plasma. If the observed beneficial effect to bulk plasma is further manifested on the condition of well-controlled EP losses, the EIC might be a very powerful tool to trigger confinement improvement of bulk plasma, similar to events induced by fishbone and toroidal Alfven eigenmode (TAE) bursts [26,27].

The authors (X. D. D. and K. T.) would like to thank A. Koenies, S. Nishimura, Y. Todo, N. Nakajima, and K. Ichiguchi for fruitful discussions. This work is in part supported by the National Institute for Fusion Science (NIFS) budget (ULPP028), the Japan Society for the Promotion of Science (JSPS) Grant-in-Aid for Scientific Research (B) 23340184 and 24360386, and the JSPS-NRF-NSFC A3 Foresight Program in the field of Plasma Physics (NSFC: No. 11261140328, NRF: No. 2012K2A2A6000443).

*Corresponding author.
du.xiaodi@lhd.nifs.ac.jp

[1] N. N. Gorelenkov, S. D. Pinches, and K. Toi, Nucl. Fusion **54**, 125001 (2014).
[2] K. McGuire *et al.*, Phys. Rev. Lett. **50**, 891 (1983).
[3] G. Matsunaga *et al.*, Phys. Rev. Lett. **103**, 045001 (2009).
[4] M. Okabayashi *et al.*, Phys. Plasmas **18**, 056112 (2011).
[5] W. W. Heidbrink *et al.*, Plasma Phys. Controlled Fusion **53**, 085028 (2011).
[6] M. S. Chu, J. Greene, L. Lao, R. Miller, A. Bondeson, O. Sauter, B. Rice, E. Strait, T. Taylor, and A. Turnbull, Phys. Rev. Lett. **77**, 2710 (1996).
[7] R. Jayakumar *et al.*, Phys. Plasmas **9**, 5043 (2002).
[8] M. Yoshinuma, K. Ida, M. Yokoyama, M. Osakabe, and K. Nagaoka, Fusion Sci. Technol. **58**, 375 (2010).
[9] M. Isobe *et al.*, Rev. Sci. Instrum. **70**, 827 (1999).
[10] Ya. I. Kolesnichenko, V. V. Lutsenko, H. Wobig, and V. Yakovenko, Phys. Plasmas **9**, 517 (2002).
[11] P. R. Goncharov, T. Ozaki, S. Sudo, N. Tamura, TESPEL Group, LHD Experimental Group, E. A. Veshchev, V. Yu. Sergeev, and A. V. Krasilnikov, Rev. Sci. Instrum. **77**, 10F119 (2006).
[12] K. Kawahata, Y. Nagayama, S. Inagaki, Y. Ito, and LHD Experimental Group, Rev. Sci. Instrum. **74**, 1449 (2003).
[13] Y. Takemura *et al.*, Plasma Fusion Res. **8**, 1402123 (2013).
[14] R. Ueda, K. Y. Watanabe, Y. Matsumoto, M. Itagaki, M. Sato, and S. Oikawa, Phys. Plasmas **21**, 052502 (2014).
[15] S. Sakakibara *et al.*, Plasma Phys. Controlled Fusion **44**, A217 (2002).
[16] S. Murakami *et al.*, Fusion Technol. **27**, 256 (1995).
[17] S. Sakakibara *et al.*, Plasma Phys. Controlled Fusion **50**, 124014 (2008).
[18] K. Ichiguchi, N. Nakajima, M. Wakatani, B. A. Carreras, and V. E. Lynch, Nucl. Fusion **43**, 1101 (2003).
[19] T. Ido, A. Shimizu *et al.*, Rev. Sci. Instrum. **77**, 10F523 (2006).
[20] N. Nakajima and M. Okamoto, J. Phys. Soc. Jpn. **60**, 4146 (1991).
[21] K. Y. Watanabe, N. Nakajima, M. Okamoto, K. Yamazaki, Y. Nakamura, and M. Wakatani, Nucl. Fusion **35**, 335 (1995).
[22] K. Itoh, S. I. Itoh, and A. Fukuyama, *Transport and Structural Formation in Plasmas* (IOP, London, 1999).
[23] K. Tanaka *et al.*, Rev. Sci. Instrum. **79**, 10E702 (2008).
[24] M. Nunami, T.-H. Watanabe, H. Sugama, and K. Tanaka, Phys. Plasmas **19**, 042504 (2012).
[25] D. R. Mikkelsen *et al.*, Phys. Plasmas **21**, 082302 (2014).
[26] S. Günter, A. Gude, J. Hobirk, M. Maraschek, S. Saarelma, S. Schade, R. C. Wolf, and ASDEX Upgrade Team, Nucl. Fusion **41**, 1283 (2001).
[27] K. Toi, K. Ogawa, M. Isobe, M. Osakabe, D. A. Spong, and Y. Todo, Plasma Phys. Controlled Fusion **53**, 024008 (2011).